Structure of the $P_{700}^{+}A_{1}^{-}$ Radical Pair Intermediate in Photosystem I by High Time Resolution Multifrequency Electron Paramagnetic Resonance: Analysis of Quantum Beat Oscillations

Gerhard Link,[†] Thomas Berthold,[†] Michael Bechtold,[†] Jörg-Ulrich Weidner,[†] Ernst Ohmes,[†] Jau Tang,[‡,§] Oleg Poluektov,[‡] Lisa Utschig,[‡] Sandra L. Schlesselman,[‡] Marion C. Thurnauer,[‡] and Gerd Kothe*[,†]

Contribution from the Department of Physical Chemistry, University of Freiburg, Albertstrasse 21, D-79104 Freiburg, Germany, and Chemistry Division, Argonne National Laboratory, 7900 South Cass Avenue, Argonne, Illinois 60439

Received September 14, 2000. Revised Manuscript Received January 16, 2001

Abstract: The geometry of the secondary radical pair, $P_{700}^{+}A_{1}^{-}$, in photosystem I (PSI) from the *deuterated* and *^{15}N-substituted* cyanobacterium *Synechococcus lividus* has been determined by high time resolution electron paramagnetic resonance (EPR), performed at three different microwave frequencies. Structural information is extracted from light-induced *quantum beats* observed in the transverse magnetization of $P_{700}^{+}A_{1}^{-}$ at early times after laser excitation. A computer analysis of the two-dimensional Q-band experiment provides the orientation of the various magnetic tensors of $P_{700}^{+}A_{1}^{-}$ with respect to a magnetic reference frame. The orientation of the cofactors of the primary donor in the **g**-tensor system of P_{700}^{+} is then evaluated by analyzing time-dependent X-band EPR spectra, extracted from a two-dimensional data set. Finally, the cofactor arrangement of $P_{700}^{+}A_{1}^{-}$ in the photosynthetic membrane is deduced from angular-dependent W-band spectra, observed for a *magnetically aligned sample*. Thus, the orientation of the **g**-tensor of P_{700}^{+} with respect to a chlorophyll based reference system could be determined. The angle between the g_1^Z axis and the chlorophyll plane normal is found to be 29 ± 7°, while the g_1^Y axis lies in the chlorophyll plane. In addition, a complete structural model for the reduced quinone acceptor, A_{1}^{-}, is evaluated. In this model, the quinone plane of A_{1}^{-} is found to be inclined by 68 ± 7° relative to the membrane plane, while the $P_{700}^{+}-A_{1}^{-}$axis makes an angle of 35 ± 6° with the membrane normal. All of these values refer to the charge separated state, $P_{700}^{+}A_{1}^{-}$, observed at *low temperatures*, where *forward electron transfer* to the iron−sulfur centers is partially blocked. Preliminary *room temperature* studies of $P_{700}^{+}A_{1}^{-}$, employing X-band *quantum beat oscillations*, indicate a different orientation of A_{1}^{-} in its binding pocket. A comparison with crystallographic data provides information on the electron-transfer pathway in PSI. It appears that *quantum beats* represent excellent structural probes for the short-lived intermediates in the primary energy conversion steps of photosynthesis.

Introduction

Spin-correlated radical pairs[1−3] are generated as short-lived intermediates in the primary energy conversion steps of photosynthesis. Charge separation in green plant photosystem I (PSI)[4,5] is initiated by photoexcitation of the primary chlorophyll donor, P_{700}. An electron is transferred from the excited singlet state of P_{700} to a phylloquinone acceptor,[6] A_1, through an intervening chlorophyll acceptor,[5] A_0. The radical pair $P_{700}^{+}A_{1}^{-}$ is the first intermediate detectable by time-resolved EPR. At *room temperature* $P_{700}^{+}A_{1}^{-}$decays in about 200 ns by *forward electron transfer* to the next acceptor,[7,8] an iron−sulfur (FeS) center.[4,5] At *low temperature*, the lifetime of $P_{700}^{+}A_{1}^{-}$ is about 150 μs, and it decays primarily by *charge recombination*.[9]

The objective of the present study is the determination of the structure of $P_{700}^{+}A_{1}^{-}$ by high time resolution electron paramagnetic resonance (EPR), performed at three different microwave frequencies. Structural information is extracted from *coherent oscillations* observed in the transverse magnetization of $P_{700}^{+}A_{1}^{-}$ at early times after laser excitation. To obtain information on the mechanism of the light-induced charge separation process, the EPR techniques are applied at two different temperatures with distinct electron-transfer kinetics. We expect that the structural data on the transient intermediates may help

* To whom correspondence should be addressed. Fax: 0049-761-203-6222. E-mail: kothe@pc1.chemie.uni-freiburg.de.

[†] University of Freiburg.

[‡] Argonne National Laboratory.

[§] Present address: Lucent Technologies, 791 Holmdel-Keyport Road, Holmdel, NJ 07733.

(1) Thurnauer, M. C.; Norris, J. R. *Chem. Phys. Lett.* **1980**, *76*, 557−561.

(2) Closs, G. L.; Forbes, M. D. E.; Norris, J. R. *J. Phys. Chem.* **1987**, *91*, 3592−3599.

(3) Buckley, C. D.; Hunter, D. A.; Hore, P. J.; McLauchlan, K. A. *Chem. Phys. Lett.* **1987**, *135*, 307−312.

(4) Golbeck, J. H.; Bryant, D. A. *Curr. Top. Bioenerg.* **1991**, *16*, 83−177.

(5) Krauss, N.; Schubert, W.-D.; Klukas, O.; Fromme, P.; Witt, H. T.; Saenger, W. *Nat. Struct. Biol.* **1996**, *3*, 965−973.

(6) Snyder, S. W.; Rustandi, R. R.; Biggins, J.; Norris J. R.; Thurnauer, M. C. *Proc. Natl. Acad. Sci. U.S.A.* **1991**, *88*, 9895−9896.

(7) Thurnauer, M. C.; Rutherford, A. W.; Norris, J. R. *Biochim. Biophys. Acta* **1982**, *682*, 332−338.

(8) Brettel, K. *FEBS Lett.* **1988**, *239*, 93−98.

(9) Sétif, P.; Mathis, P.; Vänngård, T. *Biochim. Biophys. Acta* **1984**, *767*, 404−414.

10.1021/ja003382h CCC: $20.00
Published on Web 04/14/2001

in understanding the function of the quinone acceptor in the primary electron-transfer steps of PSI.

In native PSI samples, $P_{700}^{+}A_1^{-}$ is created in a virtually pure singlet state, determined by the spin multiplicity of the excited chlorophyll donor, $^1P_{700}^{*}$. Generally, such a singlet radical pair is formed with spin-correlated population of only one-half of the eigenstates.[2,3] This gives rise to high-spin polarization, which has been exploited in structural studies of $P_{700}^{+}A_1^{-}$, using transient X- (9.5 GHz) and K-band (24 GHz) EPR.[10−12] In addition, there are *coherences* between the eigenstates of the radical pair, which can manifest themselves as *quantum beats* in an EPR experiment with adequate time resolution.[13−19] Analysis revealed, that *zero-quantum electron* and *single-quantum nuclear coherences* are involved.[19]

Previously, we have presented a high time resolution X-band study for $P_{700}^{+}A_1^{-}$, formed by photoinduced charge separation at *room temperature*.[15,16] The time evolution of the transverse magnetization was evaluated for various static magnetic fields. Manifestations of *zero quantum electron coherence* were observed at early times after laser pulse excitation.[15,16] Analyzing the fast initial oscillations, we have been able to propose the geometry of $P_{700}^{+}A_1^{-}$ in PSI at *room temperature*.[18]

Recently, the spin polarized W-band (94 GHz) EPR spectrum of $P_{700}^{+}A_1^{-}$ has been presented.[20] A qualitatively similar but different geometry for $P_{700}^{+}A_1^{-}$ has been suggested from an analysis of this spectrum, taken at *low temperature*. On the basis of this geometry good simulations of the experimental W-band and K-band spectra were obtained. [20] However, the simulation did not reproduce the X-band spectrum well.[20]

Although crystals of the PSI reaction center complex have been obtained, its three-dimensional structure is not known with sufficient detail.[5] Only very recently, the position and orientation of the reduced acceptor, A_1^{-}, could be obtained using pulsed and transient EPR in combination with PSI single crystals.[21−24] No such information is yet available for the **g**-tensor orientation of the primary donor, P_{700}^{+}.

In the following we first present a *low-temperature* transient Q-band (34 GHz) study of $P_{700}^{+}A_1^{-}$, formed by light-induced charge separation in *fully deuterated* and *^{15}N-substituted* cyanobacteria *Synechococcus lividus (S. lividus)*. *Zero quantum electron precessions* are observed in the transverse magnetization at early times after laser excitation. The phase and frequency of the *quantum beats* vary significantly across the powder spectrum. A computer analysis of the two-dimensional Q-band experiment provides the orientation of the various magnetic tensors of $P_{700}^{+}A_1^{-}$ with respect to a magnetic reference frame.

The orientation of the cofactors of the primary donor in the **g**-tensor system of P_{700}^{+} is then evaluated by analyzing time-dependent X-band EPR spectra, extracted from a two-dimensional data set taken at *low temperature*. The analysis is based on *anisotropic ^{15}N hyperfine interactions* in $P_{700}^{+}A_1^{-}$, giving rise to *nuclear modulations* in the transverse magnetization.[19] Finally, the arrangement of the cofactors of $P_{700}^{+}A_1^{-}$ in the photosynthetic membrane is deduced from angular-dependent W-band spectra, observed for a *magnetically aligned sample*.[25]

Thus, we obtain the three-dimensional structure of the short-lived radical pair intermediate $P_{700}^{+}A_1^{-}$ following photoexcitation of PSI in its native membrane. The structure, evaluated at *low temperatures*, is based on the analysis of *quantum beat oscillations* in combination with multifrequency EPR and a *magnetically oriented sample*. Preliminary *room-temperature* studies of $P_{700}^{+}A_1^{-}$, employing the same techniques, indicate a different orientation of the reduced quinone acceptor in its binding pocket. The result is discussed in relation to the distinct electron-transfer kinetics observed at *room* and *low temperature.*

Theoretical Background

In this section we briefly summarize a model for transient EPR of spin-correlated radical pairs[2,3] in photosynthetic reaction centers and define the model parameters.[13−19] In a frame rotating with the microwave frequency ω around the static magnetic field, B_0, the total spin Hamiltonian, $H(\Omega)$, of the radical pair can be written as

$$H(\Omega) = \mu_B B_0 (g_1^{zz}(\Omega) S_1^z + g_2^{zz}(\Omega) S_2^z) - \hbar\omega (S_1^z + S_2^z) + \frac{1}{2}(g_1 + g_2)\mu_B B_1 (S_1^x + S_2^x) + 2(D^{zz}(\Omega) - J_{ex}) S_1^z S_2^z - \left(\frac{1}{2} D^{zz}(\Omega) + J_{ex}\right)(S_1^- S_2^+ + S_1^+ S_2^-) + \sum_k (A_{1k}^{zz}(\Omega) S_1^z I_{1k}^z + B_{1k}(\Omega) S_1^z I_{1k}^x) + \sum_l (A_{2l}^{zz}(\Omega) S_2^z I_{2l}^z + B_{2l}(\Omega) S_2^z I_{2l}^x) + \sum_k -\mu_N g_{1k} B_0 I_{1k}^z + \sum_l -\mu_N g_{2l} B_0 I_{2l}^z \quad (1)$$

where μ_B, $g_i^{zz}(\Omega)$, $S_i^z(S_i^x)$, g_i, B_1, $D^{zz}(\Omega)$, J_{ex}, $S_i^-(S_i^+)$, $A_{ij}^{zz}(\Omega)$ ($B_{ij}(\Omega)$), $I_{ij}^z(I_{ij}^x)$,μ_N, and g_{ij} are the Bohr magneton, the *zz* component of the **g**-tensor $\mathbf{g}_i$, the $z(x)$ component of the electron spin operator $\mathbf{S}_i$, the isotropic *g*-factor of radical *i*, the strength of the microwave field, the *zz* component of the dipolar coupling tensor $\mathbf{D}(\Omega)$, the strength of the isotropic exchange interaction,[26] the lowering (raising) operator of electron *i*, the secular (pseudosecular) part of the hyperfine interaction between nucleus *j* and radical *i*,[27] the $z(x)$ component of the nuclear spin operator $\mathbf{I}_{ij}$, the nuclear magneton and the *g*-factor for nucleus *j* in radical

(10) Stehlik, D.; Bock, C. H.; Petersen, J. *J. Phys. Chem.* **1989**, *93*, 1612−1619.
(11) Füchsle, G.; Bittl, R.; van der Est, A.; Lubitz, W.; Stehlik, D. *Biochim. Biophys. Acta* **1993**, *1142*, 23−35.
(12) van der Est, A.; Sieckmann, I.; Lubitz, W.; Stehlik, D. *Chem. Phys*. **1995**, *194*, 349−359.
(13) Salikhov, K. M.; Bock, C. H.; Stehlik, D. *J. Appl. Magn. Reson.* **1990**, *1*, 195−211.
(14) Bittl, R.; Kothe, G. *Chem. Phys. Lett*. **1991**, *177*, 547−553.
(15) Kothe, G.; Weber, S.; Bittl, R.; Norris, J. R.; Snyder, S. S.; Tang, J.; Thurnauer, M. C.; Morris, A. L.; Rustandi, R. R.; Wang, Z. In *Spin Chemistry*; I'Haya, Y. J., Ed.; The Oji International Conference on Spin Chemistry: Tokyo, 1991; pp 420−434.
(16) Kothe, G.; Weber, S.; Bittl, R.; Ohmes, E.; Thurnauer, M. C.; Norris, J. R. *Chem. Phys. Lett.* **1991**, *186*, 474−480.
(17) Zwanenburg, G.; Hore, P. J. *Chem. Phys. Lett.* **1993**, *203*, 65−74.
(18) Kothe, G.; Weber, S.; Ohmes, E.; Thurnauer, M. C.; Norris, J. R. *J. Phys. Chem*. **1994**, *98*, 2706−2712.
(19) Kothe, G.; Bechtold, M.; Link, G.; Ohmes, E.; Weidner, J.-U. *Chem. Phys. Lett.* **1998**, *283*, 51−60.
(20) van der Est, A.; Prisner, T.; Bittl, R.; Fromme, P.; Lubitz, W.; Möbius, K.; Stehlik, D. *J. Phys. Chem. B* **1997**, *101*, 1437−1443.
(21) Bittl, R.; Zech, S. G.; Fromme, P.; Witt, H. T.; Lubitz, W. *Biochemistry* **1997**, *36*, 12001−12004.
(22) Schubert, W.-D.; Klukas, O.; Krauss, N.; Saenger, W.; Fromme, P.; Witt, H. T. *J. Mol. Biol.* **1997**, *272*, 741−769.
(23) Kamlowski, A.; Zech, S. G.; Fromme, P.; Bittl, R.; Lubitz, W.; Witt, H. T.; Stehlik, D. *J. Phys. Chem. B.* **1998**, *102*, 8266−8277.
(24) Klukas, O.; Schubert, W.-D.; Jordan, P.; Krauss, N.; Fromme, P.; Witt, H. T.; Saenger, W. *J. Biol. Chem.* **1999**, *274*, 7361−7367. Protein Data Bank of Brookhaven National Laboratory, 1C51.pdb, October 1999.
(25) Berthold, T.; Bechtold, M.; Heinen, U.; Link, G.; Poluektov, O.; Utschig, L.; Tang, J.; Thurnauer, M. C.; Kothe, G. *J. Phys. Chem. B* **1999**, *103*, 10733−10736.
(26) The sign of the exchange interaction parameter, J_{ex}, has been chosen to common practice.
(27) Reitz, D. C.; Weissman, S. I. *J. Chem. Phys.* **1960**, *33*, 700−704.

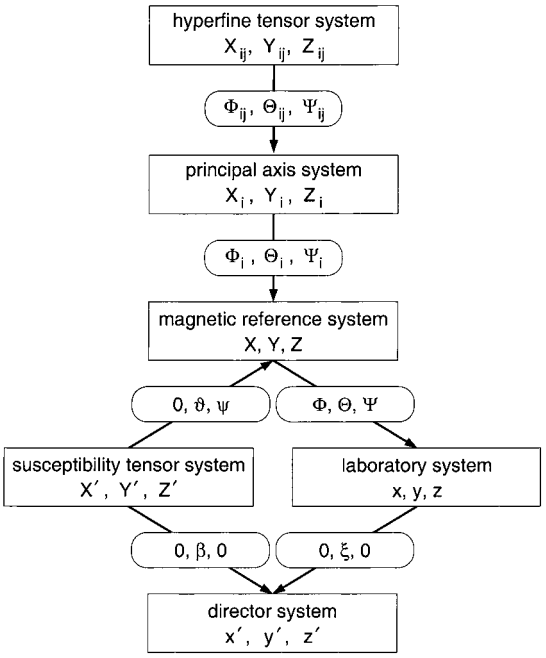

Figure 1. Notation for coordinate systems and Euler transformations used in the EPR model. $\mathbf{X}_i$, $\mathbf{Y}_i$, $\mathbf{Z}_i$ = principal axis system of the dipolar tensor (i = D) and of the **g**-tensor of the primary donor (i = 1). **X**, **Y**, **Z** = magnetic reference system (**g**-tensor of the reduced quinone acceptor). **z** = magnetic field direction, **Z′** = symmetry axis of the susceptibility tensor (membrane normal), **z′** = director axis (net ordering axis).

i, respectively. The orientation dependence of the magnetic tensor elements $g_i^{zz}(\Omega)$ and $D^{zz}(\Omega)$ can be evaluated by a two-fold transformation from the corresponding principal axis system, $\mathbf{X}_i$, $\mathbf{Y}_i$, $\mathbf{Z}_i$,(g_i^j and D^j, $j = X, Y, Z$). In the first step we transform to a molecular reference system, **X**, **Y**, **Z**, using the Euler angles,[28] $\Omega_i = (\Phi_i, \Theta_i, \Psi_i)$. In the second step we transform by the Euler angles $\Omega = (\Phi, \Theta, \Psi)$ in the laboratory frame, **x**, **y**, **z** (see Figure 1). Evaluation of the tensor elements $A_{ij}^{zz}(\Omega)$ and $B_{ij}(\Omega)$ requires an additional transformation from the principal axis system, $\mathbf{X}_{ij}$, $\mathbf{Y}_{ij}$, $\mathbf{Z}_{ij}$, (A_{ij}^k, $k = X, Y, Z$), of the respective hyperfine tensor to the principal axis system, $\mathbf{X}_i$, $\mathbf{Y}_i$, $\mathbf{Z}_i$, of the **g**-tensor $\mathbf{g}_i$ (see Figure 1).

In native photosynthetic reaction centers the secondary radical pairs are generated in a virtually pure singlet state, determined by the spin multiplicity of the excited chlorophyll donor.[13−19] Generally, such a singlet radical pair is created with spin-correlated populations of only one-half of the eigenstates[2,3] and with *zero quantum electron coherence*[13−19] and *single quantum nuclear coherence*[19,29−31] between these states. In the absence of a microwave field, the eigenstate populations are constant in time, while the *zero quantum electron* and *nuclear coherences* oscillate at distinct frequencies, given by the energy separation of the corresponding eigenstates.[19] The continuous microwave field, applied in transient EPR, has two effects. First, it converts the longitudinal magnetization associated with the population differences between neighboring eigenstates into transverse magnetization.[17,32] This gives the Torrey oscillations virtually independent of B_0.[17,32] Second, it converts the *zero quantum electron* and *nuclear coherences* into observable single quantum precessions or *quantum beats*,[13−19] significantly varying with B_0.[14,16,18]

Under solid-state conditions, the frequency ω_{ZQ} of the *zero quantum electron precessions* critically depends on the orientation, Ω, of the radical pair in the laboratory frame. The weak B_1 field, commonly employed in transient EPR, allows for only a small range of orientations to meet the resonance condition. Consequently, the phase and frequency of the *quantum beats* vary significantly with B_0 across the powder spectrum. This pronounced variation can be used to extract the geometry of radical pair intermediates in photosynthetic reaction centers.[16,18,33,34] In deriving eq 2

$$\omega_{ZQ} = (1/\hbar)\{[{}^2/_3 D^{zz}(\Omega) - 2J_{ex}]^2 + [(g_1^{zz}(\Omega) - g_2^{zz}(\Omega))\mu_B B_0 + \sum_k A_{1k}^{zz}(\Omega)M_{1k}^i - \sum_l A_{2l}^{zz}(\Omega)M_{2l}^j]^2\}^{1/2}$$
$$M_{1k}^i = I_{1k}, I_{1k} - 1, \ldots, -I_{1k}$$
$$M_{2l}^j = I_{2l}, I_{2l} - 1, \ldots, -I_{2l} \quad (2)$$

all pseudosecular terms of the hyperfine interactions have been neglected. As a result, *light-induced nuclear coherences*[19,29−31] are not considered in the analysis. The latter is certainly a good approximation for Q- and W-band studies, since the modulation depth of these coherences decreases strongly with the applied magnetic field.[19] For the analysis of X-band experiments, however, consideration of *anisotropic hyperfine interactions* is essential.[19]

Integrating the time-dependent transverse magnetization of the radical pair over an appropriate time window and plotting this integral as a function of B_0 yields the transient EPR spectrum. High-field EPR experiments on photosynthetic reaction centers, frozen in the presence of the strong magnetic field, indicate an *anisotropic distribution* of the radical pair with respect to the laboratory frame.[25] The physical origin of this effect is an anisotropy in the diamagnetic susceptibility of the reaction center protein. If we make the simplifying assumption that the susceptibility tensor is axially symmetric in its principal axis system, **X′**, **Y′**, **Z′** (see Figure 1), the *orientational distribution function* of the reaction centers can be written as:[25]

$$f(\beta) = N' \exp(A \cos^2 \beta) \quad (3)$$

Here N' is a normalization constant, and β denotes the angle between the symmetry axis of the susceptibility tensor and the director axis (net ordering axis), **z′** (see Figure 1). The coefficient A characterizes the *magnetic field induced alignment* of the reaction centers along **z′**, while the angle ξ specifies the orientation of **z′** in the laboratory frame (see Figure 1). The orientational order parameter, $S_{Z'Z'}$, is related to the coefficient A by a mean value integral.[25] Since the principal axis of the susceptibility tensor, **Z′**, has a fixed orientation, ϑ, ψ, with respect to a magnetic reference system (see Figure 1), it is possible to express cosβ as a function of Φ, Θ, Ψ, and ξ.[25] Thus, one obtains the *orientational distribution function* of the radical pair with respect to the laboratory frame.

(28) Edmonds, A. R. *Angular Momentum in Quantum Mechanics*; Princeton University Press: Princeton, 1974; pp 6−8.
(29) Weber, S.; Ohmes, E.; Thurnauer, M. C.; Norris, J. R.; Kothe, G. *Proc. Natl. Acad. Sci. U.S.A.* **1995**, *92*, 7789−7793.
(30) Weber, S.; Kothe, G.; Norris, J. R. *J. Chem. Phys.* **1997**, *106*, 6248−6261.
(31) Jeschke, G. *J. Chem. Phys.* **1997**, *106*, 10072−10086.
(32) Gierer, M.; van der Est, A.; Stehlik, D. *Chem. Phys. Lett.* **1991**, *186*, 238−247.
(33) Kothe, G.; Weber, S.; Ohmes, E.; Thurnauer, M. C.; Norris, J. R. *J. Am. Chem. Soc.* **1994**, *116*, 7729−7734.
(34) Kiefer, A. M.; Kast, S. M.; Wasielewski, M. R.; Laukenmann, K.; Kothe, G. *J. Am. Chem. Soc.* **1999**, *121*, 188−198.

Materials and Methods

Sample Preparation. Lyophilized, whole cells of *deuterated* (99.7%) and *^{15}N-substituted* (95%) cyanobacteria *S. lividus* were rehydrated in deuterated Tris buffer (uncorrected pH = 7.5), containing 50% glycerol as cryoprotection. The suspension was then placed in a quartz tube (2 mm i.d.) or quartz capillary (0.9 mm o.d., 0.5 mm i.d.), located in the symmetry axis of the microwave resonator. *Magnetic-field induced alignment* of the photosynthetic reaction centers was achieved at room temperature with the field of the EPR spectrometer.[25] The sample was then cooled to low temperatures, and the EPR spectra were measured as a function of the angle ξ between the director axis and magnetic field.

X- and Q-Band EPR Measurements. The time-resolved EPR experiments were carried out using a transient X- or Q-band bridge in combination with a Bruker ESP300E console. The field of the water-cooled magnet was calibrated against Li:LiF (Institute of Crystallography, Moscow), which is a good standard for low-temperature measurements.[35] The transient X-band bridge (Bruker ER046MRT) was equipped with a fast low-noise preamplifier and a broad band video amplifier (bandwidth 200 Hz to 200 MHz). Irradiation of the sample was performed in a home-built split-ring resonator, exhibiting a high filling factor at low Q (unloaded $Q \approx 300$). The Q-band experiments were carried out using a newly developed transient Q-band bridge (Bruker ER050QGT). The sample was irradiated in a cylindrical cavity with a loaded Q of approximately 700, corresponding to a bandwidth of 50 MHz. A frequency counter (HP5352B) was used to monitor the microwave frequency in the X- and Q-band range.

For optical excitation the frequency-doubled output of a Nd:YAG laser (Spectra Physics Quanta Ray GCR190-10) with a wavelength of 532 nm and a pulse width of 2.5 ns was used. For the actual experiment the intensity was attenuated to approximately 2 mJ/pulse. To avoid photoselection, the laser beam was passed through a quartz depolarizer. The repetition rate of the laser was 10 Hz. A transient recorder (LeCroy 9354A) with a maximum digitizing rate of 1 ns/11 bit sample was used to acquire the time-dependent EPR signal. The transients were accumulated at off-resonance conditions and subtracted from those on resonance to get rid of the laser background signal.

W-Band EPR Measurements. The high-field experiments were carried out on a Bruker ELEXSYS E680X W-band EPR spectrometer, equipped with a TE_{011} cylindrical cavity and high bandwidth mixer detection. The field of the superconducting magnet was calibrated using Li:LiF (Institute of Crystallography, Moscow) as a standard.[35] Optical excitation of the sample was performed with 2.5 ns pulses of a Q-switched, frequency-doubled Nd:YAG laser (Spectra Physics Quanta Ray GCR130-15). The laser output was depolarized and attenuated to approximately 1 mJ/pulse. Excitation of the sample in the resonator was achieved using a fiber-optic light path through the sample rod (silica optical fiber, 400 μm core diameter, Fiberguide Industries), as described previously.[36] The time-resolved EPR signal was recorded and averaged with a LeCroy 9354A digital oscilloscope. Typically, 400 transients were accumulated to improve the signal/noise ratio. A weak chlorophyll triplet signal, superimposed on the radical pair signal, was subtracted using a linear interpolation procedure.

Computations. A Fortran program package,[37,38] based on the theoretical approach outlined in the previous section, was employed to analyze the time-resolved EPR experiments. The programs calculate EPR time profiles and transient spectra of spin-correlated radical pairs with a spatially fixed geometry. *Anisotropic hyperfine interactions*, including pseudosecular terms for the ^{15}N nuclei, were explicitly taken into account in the analysis of X-band data.[38] The corresponding diagonalizations were accomplished by using the Rutishauser algorithm according to Gordon and Messenger.[39] Fortran routines were taken from the literature[39−41] and modified for this purpose. The structural parameters were evaluated using a nonlinear least-squares fit procedure based on the Levenberg−Marquardt algorithm.[42] Generally, a representative set of calculated time profiles was simultaneously fitted to the experimental profiles by varying the geometry parameters. The uniqueness of the fit was tested by running the fit procedure with different experimental data sets and different starting values.

Experimental Results

The objective of this study is the structural characterization of a radical pair intermediate in PSI. To achieve this goal, suspensions of *deuterated* and *^{15}N-substituted* cyanobacteria *S. lividus* were irradiated with 2.5 ns pulses from a Nd:YAG laser, and the time evolution of the transverse magnetization was monitored at three different microwave frequencies. Typical X-, Q- and W-band results are shown in Figures 2−6. The observed time profiles and transient spectra vary drastically according to the microwave frequency band employed.

Transient Q-Band Data Set. Generally, a complete EPR data set consists of transient signals taken at equidistant field points covering the total spectral width. This yields a two-dimensional variation of the signal intensity with respect to both the magnetic field and the time axis. Transient spectra can be extracted from such a plot at any time after the laser pulse as slices parallel to the magnetic field axis. Likewise, the time evolution of the transverse magnetization may be obtained for any given field as a slice along the time axis.

Typical Q-band line shapes, observed 20, 40, and 160 ns after the laser pulse, are shown in Figure 2 (solid lines). The spectra refer to a microwave frequency of $\omega/2\pi = 33.9893$ GHz, $B_1 = 0.029$ mt and $T = 70$ K. Note that a positive signal indicates absorptive (a) and a negative emissive (e) spin polarization. Apparently, the early spectrum is much broader than the later ones. Moreover, the polarization changes from a simple e/a/e/(a) pattern at early times to a characteristic e/a/a/e/a pattern at later times. It can be assigned to the secondary radical pair, $P_{700}^{+}A_1^{-}$.

Figures 3 and 4 depict the short time behavior of the transverse magnetization (solid lines) measured at eight selected field positions (A−H, Figure 2). Evidently, there are fast initial oscillations which disappear 100 ns after the laser pulse. Note that the frequency of these oscillations varies significantly across the powder spectrum. Generally, oscillation frequencies from 10 to 50 MHz can be extracted from the corresponding power spectra. Basically, these oscillations represent Q-band *quantum beats*,[34] associated with the spin-correlated generation of the radical pair (see eq 2).

Transient X-Band Spectra. Despite the excellent spectral resolution, transient Q-band EPR cannot provide all of the desired structural information. It is therefore necessary to extend the studies to the X-band regime, where *anisotropic hyperfine interactions* play a major role. Typical X-band line shapes, observed 50, 100, and 200 ns after the laser pulse, are shown in Figure 5a (solid lines). The spectra refer to a microwave frequency of $\omega/2\pi = 9.57375$ GHz, $B_1 = 0.020$ mT and $T = 70$ K. One sees that the early spectrum is much broader than the latter ones, which we attribute to lifetime broadening.[43]

(35) Cherkasov, F. G.; Denisenko, G. A.; Vitol, A. Ya.; L'vov, S. G. In *Proceedings of the XXVIIth Congress Ampère on Magnetic Resonance and Related Phenomena;* Salikhov, K. M., Ed.; Zavoisky Physical-Technical Institute Kazan, 1994; Vol. 1, pp 416−417.

(36) Hofbauer, W.; Bittl, R. *Bruker Report* **1998**, *145*, 38−39.

(37) Laukenmann, K. Ph.D. Thesis, University of Freiburg, 1999.

(38) Link, G.; Weidner, J.-U.; Kothe, G. Manuscript in preparation.

(39) Gordon, R. G.; Messenger, T. In *Electron Spin Relaxation in Liquids*; Muus, L. T., Atkins, P. W., Eds.; Plenum Press: New York, 1972; pp 341−381.

(40) Cullum, J.; Willoughby, R. A. *Lanczos Algorithms for Large Symmetric Eigenvalue Computations*; Birkenhäuser: Basel, 1985; Vol. 2.

(41) Smith, B. T.; Boyle, J. M.; Dongarra, J. J.; Garbow, B. S.; Ikebe, Y.; Klema, V. C.; Moler, C. B. In *Lecture Notes in Computer Science*; Goos, G., Hartmanis, J., Eds.; Springer: Berlin, Heidelberg, New York, 1976; Vol. 6.

(42) Press: W. H.; Teukolsky, S. A.; Vetterling, W. T.; Flannery, B. P. *Numerical Recipes in Fortran*; Cambridge University Press: Cambridge, 1992.

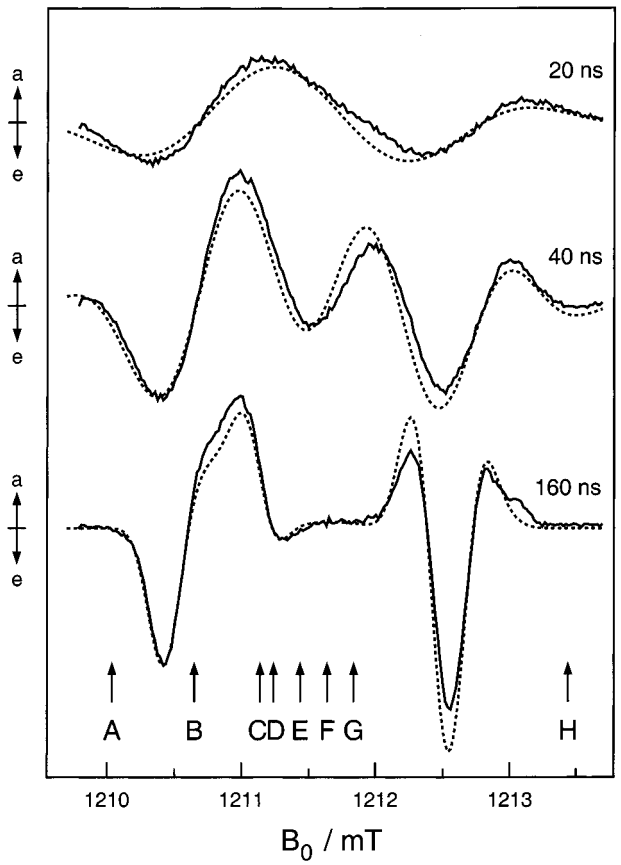

Figure 2. Transient Q-band EPR spectra of the light-induced radical pair, $P_{700}^{+}A_1^{-}$, in photosystem I at various times after the laser pulse. Positive and negative signals indicate absorptive and emissive polarizations, respectively. Microwave field, $B_1 = 0.029$ mT. Microwave frequency, $\omega/2\pi = 33.9893$ GHz. Full lines: Experimental spectra from the *deuterated* and *^{15}N-substituted* cyanobacterium *Synechococcus lividus*. Temperature, $T = 70$ K. Dashed lines: Calculated spectra using the parameters given in Table 1. Various field positions are marked from A to H. The time evolution of the transverse magnetization at those field positions is shown in the Figures 3 and 4.

Moreover, the spectral shape changes significantly with time. The characteristic e/a/e/(a) pattern, observed at later times, is in agreement with results made on similar PSI preparations under comparable experimental conditions.[19,29] Note, however, that the low-field emissive peak is stronger than the high-field one, in contrast to observations at *room temperature*.[16,18]

Transient W-Band Spectra. High-field EPR spectra from PSI reaction centers, frozen in the presence of the magnetic field, indicate an *anisotropic distribution* of the radical pair with respect to the laboratory frame.[25] Typical results are shown in Figure 6. The transient W-band spectra, averaged in the time window 0.4−2.4 μs, refer to a microwave frequency of $\omega/2\pi = 94.1163$ GHz, $B_1 = 0.01$ mT and $T = 90$ K. To establish any *field-induced alignment* of the reaction centers, the line shapes were taken at two different orientations of the frozen sample. The left-hand EPR spectrum (solid line, Figure 6a) reflects the original sample orientation immediately after cooling ($\xi = 0°$). For the right-hand spectrum (solid line, Figure 6b), the frozen sample was rotated by 90° about an axis perpendicular to the magnetic field ($\xi = 90°$). Pronounced spectral differences are observed particularly in the high-field region. If, however, the sample was cooled in the absence of the magnetic field, two identical line shapes were detected (results not shown).

Evidently, the PSI reaction centers of *S. lividus* cyanobacteria have been aligned in the static magnetic field of the W-band spectrometer, as expected on theoretical grounds.[44] The alignment, confirmed by a recent D-band (130 GHz) study of *S. lividus* cyanobacteria,[45] corresponds to previous observations for other photosynthetic systems. Using fluorescence polarization and linear dichroism measurements, *magneto-orientation* could be established for whole cells of various green algae.[46]

Structure Determination

Strategy of Data Analysis. The new structural information on the radical pair $P_{700}^{+}A_1^{-}$ can only be derived with the data obtained at three microwave frequencies. The strategy is as follows: The orientation of the magnetic tensors of $P_{700}^{+}A_1^{-}$ is obtained from analysis of the pronounced anisotropy of the *zero quantum electron coherences* in the transient *Q-band* EPR experiment. The orientation of the cofactors of the primary donor is then determined by analyzing transient *X-band* EPR spectra, extracted from a two-dimensional data set. Finally, the transient *W-band* spectra of the *magnetically aligned sample* provide detailed information on the cofactor arrangement of $P_{700}^{+}A_1^{-}$ in the photosynthetic membrane.

Orientation of the Magnetic Tensors. The orientation of the magnetic tensors of $P_{700}^{+}A_1^{-}$ (**g**-tensors, dipolar tensor) with respect to a magnetic reference system was obtained from a computer analysis of the two-dimensional Q-band experiment (see Figures 2−4). The underlying magnetic parameters are summarized in Table 1. The **g**-tensor components of P_{700}^{+} and A_1^{-} were adapted from recent high-field EPR studies of various PSI preparations.[20,47,48] The listed spin−spin coupling parameters are based on electron spin−echo envelope modulation (ESEEM) studies of $P_{700}^{+}A_1^{-}$.[49] Hyperfine interactions in the radical pair were *approximated* by considering eight equivalent ^{15}N nuclei in P_{700}^{+} ($a_N = 0.077$ mT) and four equivalent ^{2}H nuclei ($a_D = 0.055$ mT) in A_1^{-}. This corresponds to second moments of $\langle B_0^2 \rangle = 1.19 \times 10^{-2}$ mT^2 and $\langle B_0^2 \rangle = 0.81 \times 10^{-2}$ mT^2,[50] in agreement with published hyperfine parameters for P_{700}^{+} and A_1^{-} (see Table 3). Note that the neglect of *anisotropic hyperfine interactions* is generally a good approximation for Q-band studies (see Theory section).[19]

The mutual orientation of the magnetic tensors in $P_{700}^{+}A_1^{-}$ was determined from the B_0 dependence of the Q-band *quantum beats*. Typically, a set of 22 calculated time profiles, covering the total spectral width, was simultaneously fitted to the experimental profiles by varying the parameters of the tensor orientations. In the calculations, the limited resonator bandwidth of 50 MHz was considered by using a Gaussian response function. Similarly, inhomogeneous broadening was taken into account by convolution with a Gaussian of line width $\Delta B_0 = 0.12$ mT.[51] Finally, spin relaxation was considered by multiplying each time profile by an exponential decay curve, characterized by the spin−spin relaxation time T_2. The values for T_2 vary slightly across the powder spectrum, exhibiting $T_2 \approx 1.2$ μs at position A. In Figures 3 and 4 we compare experimental (solid lines) and fitted time profiles (dashed lines) at early times after

(43) Furrer, R.; Thurnauer, M. C. *Chem. Phys. Lett.* **1981**, *79*, 28−33.
(44) Worcester, D. L. *Proc. Natl. Acad. Sci. U.S.A.* **1978**, *75*, 5475−5477.
(45) Poluektov, O.; Heinen, U.; Kothe, G.; Thurnauer, M. C. Unpublished results.
(46) Geacintov, N. E.; van Nostrand: F.; Becker, J. F.; Tinkel, J. B. *Biochim. Biophys. Acta* **1972**, *267*, 65−79.
(47) Bratt, P. J.; Rohrer, M.; Krystek, J.; Evans, M. C.; Brunel, L.-C.; Angerhofer, A. *J. Phys. Chem. B* **1997**, *101*, 9686−9689.
(48) McMillan, F.; Hanley, J.; van der Weerd, L.; Küpling, M.; Un, S.; Rutherford, A. W. *Biochemistry* **1997**, *36*, 9297−9303.
(49) Bittl, R.; Zech, S. *J. Phys. Chem. B* **1997**, *101*, 1429−1436.
(50) Vincow, G.; Johnson, P. M. *J. Chem. Phys.* **1963**, *39*, 1143−1153.

Table 1. Magnetic and Structural Parameters Used in the Simulation of Transient Q-Band EPR Experiments of the Light-Induced Radical Pair, $P_{700}^{+}A_1^{-}$, in Deuterated and ^{15}N-Substituted Photosystem I

microwave field	**g**-tensor components[a]		spin−spin coupling[b]	hyperfine interactions[c]		line broadening,[d] relaxation[e]	$\mathbf{g}_1$-tensor orientation[f]	dipolar tensor orientation[f]
	P_{700}^{+}	A_1^{-}		P_{700}^{+}	A_1^{-}			
$\omega/2\pi$ 33.9893 GHz	g_1^X, 2.00311	g_2^X, 2.00624	D, −0.17 mT	eight ^{15}N nuclei	four ^{2}H nuclei	ΔB_0, 0.12 mT	Φ_1, 176 ± 6°	Φ_D, arbitr.
B_1, 0.029 mT	g_1^Y, 2.00256	g_2^Y, 2.00510	E, 0 mT	a_N, 0.077 mT	a_D, 0.055 mT	T_2, 1.2−1.4 μs	Θ_1, 50 ± 3°	Θ_D, 78 ± 2°
	g_1^Z, 2.00230	g_2^Z, 2.00220	J_{ex}, 0 mT				Ψ_1, 64 ± 5°	Ψ_D, 16 ± 3°

[a] Data from high-field EPR studies.[20,47,48] [b] Parameter values from a recent ESEEM study of $P_{700}^{+}A_1^{-}$.[49] [c] Isotropic hyperfine interactions corresponding to second moments of $\langle B_0^2\rangle = 1.19 \times 10^{-2}$ mT^2 and $\langle B_0^2\rangle = 0.81\times10^{-2}$ mT^2. [d] Inhomogeneous broadening is considered by convolution with a Gaussian of line width $\Delta B_0 = 0.12$ mT.[51] [e] The homogeneous spin−spin relaxation T_2 has been estimated from the decay of the transient nutations. [f] Evaluated in the present study from the B_0-dependence of Q-band quantum beat oscillations. The Euler angles[28] relate the principal axis system of the respective magnetic tensor and the magnetic reference system (**g**-tensor of A_1^{-}). The cited errors are linear confidence limits (confidence level 0.95).

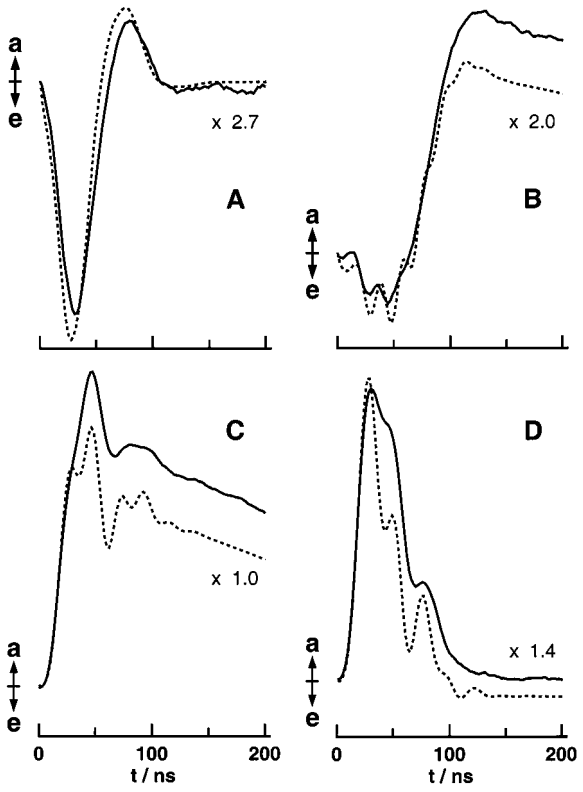

Figure 3. Time evolution of the transverse magnetization of the light-induced radical pair, $P_{700}^{+}A_1^{-}$, in photosystem I immediately after the laser pulse. The transients refer to four different static magnetic fields (positions A−D, Figure 2). Positive and negative signals indicate absorptive and emissive polarizations, respectively. Microwave field, $B_1 = 0.029$ mT. Microwave frequency, $\omega/2\pi = 33.9893$ GHz. Full lines: Experimental time profiles from the *deuterated* and *^{15}N-substituted* cyanobacterium *Synechococcus lividus*. Temperature, $T =$ 70 K. Dashed lines: Calculated time profiles using the parameters given in Table 1.

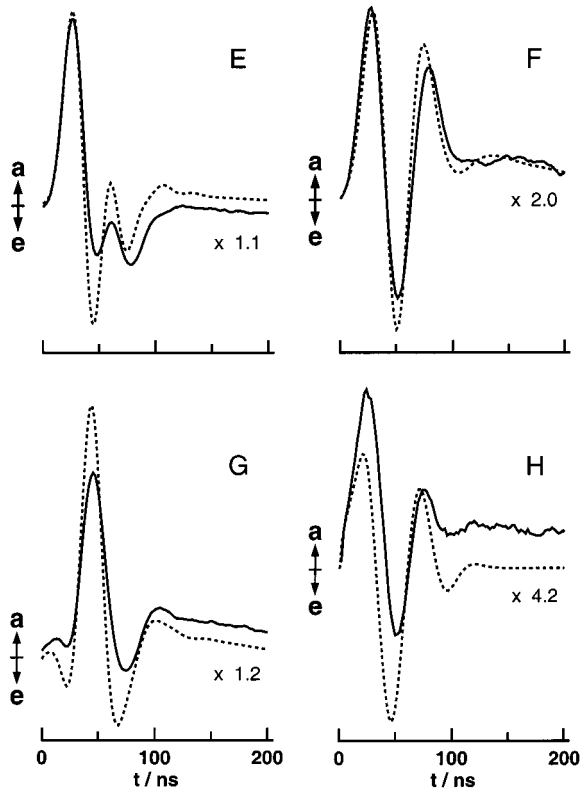

Figure 4. Time evolution of the transverse magnetization of the light-induced radical pair, $P_{700}^{+}A_1^{-}$, in photosystem I immediately after the laser pulse. The transients refer to four different static magnetic fields (positions E−H, Figure 2). Positive and negative signals indicate absorptive and emissive polarizations, respectively. Microwave field, $B_1 = 0.029$ mT. Microwave frequency, $\omega/2\pi = 33.9893$ GHz. Full lines: Experimental time profiles from the *deuterated* and *^{15}N-substituted* cyanobacterium *Synechococcus lividus*. Temperature, $T =$ 70 K. Dashed lines: Calculated time profiles using the parameters given in Table 1.

the laser pulse. Generally, the agreement achieved is good. This is true, also for the time-dependent line shapes, shown in Figure 2. Nevertheless, some deviations still exist. They may be caused by the limited resonator bandwidth. The uniqueness of the fit was tested by running the fit procedure with different experimental data sets and different starting values. Within the error limits, the same or magnetically equivalent tensor orientations were obtained. Thus, we conclude that the underlying geometry, characterized by the five Euler angles,

$$\Phi_1 = 176 \pm 6°, \quad \Theta_1 = 50 \pm 3°, \quad \Psi_1 = 64 \pm 5°,$$
$$\Phi_D = 78 \pm 2°, \quad \Psi_D = 16 \pm 3°$$

is basically correct. Note that these Euler angles[28] relate the principal axis system of the respective magnetic tensor (**g**-tensor of P_{700}^{+}, dipolar tensor) and the magnetic reference system, collinear with the **g**-tensor of A_1^{-} (see Table 1). The cited errors are linear confidence limits, referring to a confidence level of 0.95.

Orientation of the Cofactors. The cofactor orientation of the primary donor in the **g**-tensor system of P_{700}^{+} was determined by analyzing transient X-band EPR spectra (see Figure 5), extracted from a two-dimensional data set. However, in contrast to the Q-band study, *anisotropic ^{15}N and ^{2}H hyperfine interactions* were explicitly taken into account.

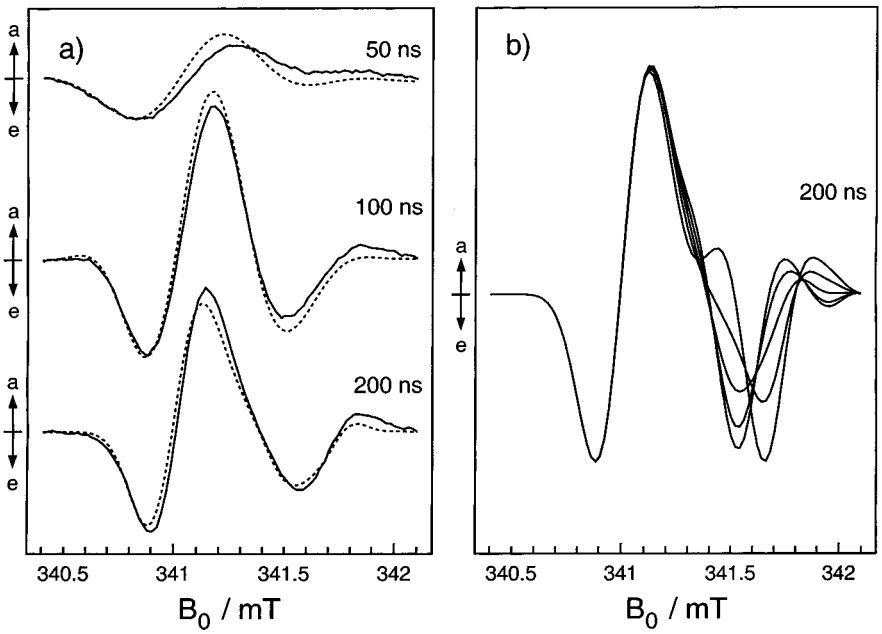

Figure 5. Transient X-band spectra of the light-induced radical pair, $P_{700}^{+}A_1^{-}$, in photosystem I at various times after the laser pulse. Positive and negative signals indicate absorptive and emissive polarizations, respectively. Microwave field, $B_1 = 0.020$ mT. Microwave frequency, $\omega/2\pi = 9.57375$ GHz. (a) Full lines: Experimental spectra from the *deuterated* and ^{15}*N-substituted* cyanobacterium *Synechococcus lividus*. Temperature, $T = 70$ K. Dashed lines: Calculated spectra using the parameters given in Tables 2 and 3. (b) Calculated line shapes for different orientations of the symmetry axis of the ^{15}N hyperfine tensors in the **g**-tensor system of P_{700}^{+}. The spectra refer to a fixed value of Θ_{1j} and five different values of Ψ_{1j}, i.e., $\Theta_{1j} = 30°$ and $\Psi_{1j} = -60°, -30°, 0°, 30°, 60°$.

Table 2. Magnetic and Structural Parameters Used in the Simulation of Transient X-Band EPR Experiments of the Light-Induced Radical Pair, $P_{700}^{+}A_1^{-}$, in Deuterated and ^{15}N-Substituted Photosystem I

microwave field	**g**-tensor components[a]		spin−spin coupling[b]	line broadening,[c] relaxation[d]	$\mathbf{g}_1$-tensor orientation[e]	dipolar tensor orientation[e]
	P_{700}^{+}	A_1^{-}				
$\omega/2\pi$ 9.57375 GHz	g_1^X, 2.00311	g_2^X, 2.00624	D, −0.17 mT	ΔB_0, 0.12 mT	Φ_1, 176°	Φ_D, arbitr.
B_1, 0.020 mT	g_1^Y, 2.00256	g_2^Y, 2.00510	E, 0 mT	T_2, 1.7μs	Θ_1, 50°	Θ_D, 78°
	g_1^Z, 2.00230	g_2^Z, 2.00220	J_{ex}, 0 mT		Ψ_1, 64°	Ψ_D, 16°

[a] Data from high-field EPR studies.[20,47,48] [b] Parameter values from a recent ESEEM study of $P_{700}^{+}A_1^{-}$.[49] [c] Inhomogeneous broadening is considered by convolution with a Gaussian of line width $\Delta B_0 = 0.12$ mT.[51] [d] The homogeneous spin−spin relaxation T_2 has been estimated from the decay of the transient nutations. [e] Evaluated in the present study from the B_0-dependence of Q-band quantum beat oscillations. The Euler angles[28] relate the principal axis system of the respective magnetic tensor and the magnetic reference system (**g**-tensor of A_1^{-}).

Table 3. Hyperfine Interaction Parameters Used in the Simulation of Transient X-Band EPR Experiments of the Light-Induced Radical Pair, $P_{700}^{+}A_1^{-}$, in Deuterated and ^{15}N-Substituted Photosystem I

^{2}H nuclei in A_1^{-}				^{15}N nuclei in P_{700}^{+}				
methyl deuterons (3)		hydrogen bond		chlorophyll couplings (4)				
tensor comp.[a]	tensor orient.[b]	tensor comp.[a]	tensor orient.[c]	tensor components[d]				tensor orient.[e]
A_{21}^X, 0.049 mT	Φ_{21}, arbitr.	A_{22}^X, −0.030 mT	Φ_{22}, arbitr.	A_{11}^X, 0.087 mT	A_{12}^X, 0.082 mT	A_{13}^X, 0.078 mT	A_{14}^X, 0.064 mT	Φ_{1j}, arbitr.
A_{21}^Y, 0.049 mT	Θ_{21}, 90°	A_{22}^Y, −0.030 mT	Θ_{22}, 120°	A_{11}^Y, 0.087 mT	A_{12}^Y, 0.082 mT	A_{13}^Y, 0.078mT	A_{14}^Y, 0.064 mT	Θ_{1j}, 29 ± 7°
A_{21}^Z, 0.070 mT	Ψ_{21}, 60°	A_{22}^Z, 0.074 mT	Ψ_{22}, 240°	A_{11}^Z, 0.155 mT	A_{12}^Z, 0.095 mT	A_{13}^Z, 0.165mT	A_{14}^Z, 0.183 mT	Ψ_{1j}, 3 ± 6°

[a] Adapted from a proton ENDOR study.[52] [b] Adapted from a transient EPR study of $P_{700}^{+}A_1^{-}$ in PSI single crystals.[23] The Euler angles[28] relate the symmetry axis of the ^{2}H hyperfine tensor and the **g**-tensor of A_1^{-}. [c] Extracted from transient X-band spectra of $P_{700}^{+}A_1^{-}$ using a protonated sample.[54] The Euler angles[28] relate the symmetry axis of the ^{2}H hyperfine tensor and the **g**-tensor of A_1^{-}. [d] Data from a recent ENDOR and ESEEM study.[55] [e] Evaluated in the present study from time-dependent X-band spectra. The Euler angles[28] characterize the orientation of the symmetry axis of the ^{15}N hyperfine tensors in the **g**-tensor system of P_{700}^{+}. The cited errors are linear confidence limits (confidence level 0.95).

Table 2 summarizes the magnetic and structural parameters used in the X-band simulations. One sees that the **g**-tensor components[20,47,48] and spin−spin coupling parameters[49] are the same as those employed in the analysis of the Q-band experiment. This is true, also for the orientation of the magnetic tensors, evaluated in the previous section. *Anisotropic hyperfine interactions* in A_1^{-} were considered by using published proton hyperfine tensors.[52] The corresponding parameters are summarized in Table 3. The orientation of the methyl group in the **g**-tensor system of A_1^{-} was adapted from a single-crystal EPR study of $P_{700}^{+}A_1^{-}$.[23] Basically, this orientation corresponds to the assignment of the **g**-tensor axes in the benzosemiquinone

(51) Fessmann, N.; Rösch, E.; Ohmes, E.; Kothe, G. *Chem. Phys. Lett.* **1988**, *152*, 491−496.
(52) Rigby, S. E. J.; Evans, M. C. W.; Heathcote, P. *Biochemistry* **1996**, *35*, 6651−6656.

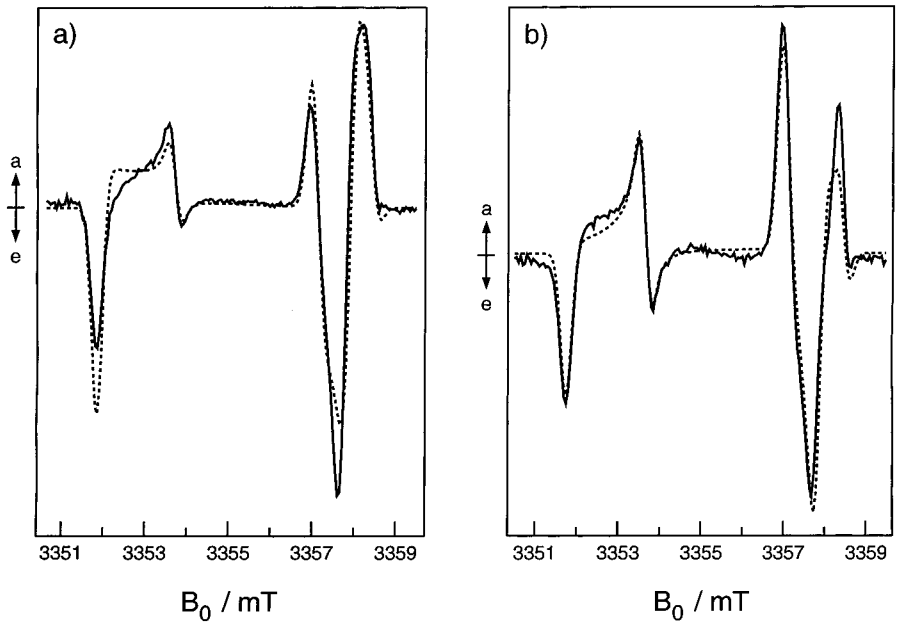

Figure 6. Transient W-band EPR spectra of the light-induced radical pair, $P_{700}^{+}A_1^{-}$, in photosystem I at two different orientational distributions with respect to the laboratory frame. Positive and negative signals indicate absorptive and emissive polarizations, respectively. (a) Director parallel to the magnetic field, $\xi = 0°$. (b) Director perpendicular to the magnetic field, $\xi = 90°$. Microwave frequency, $\omega/2\pi = 94.1163$ GHz. Full lines: Experimental spectra from the *deuterated* and *^{15}N-substituted* cyanobacterium *Synechococcus lividus*, cooled to 90 K in the *presence* of the static magnetic field of 3.35 T. Microwave field, $B_1 = 0.01$ mT. The signal intensity was averaged in the time window 0.4−2.4 μs. Dashed lines: Calculated spectra using the parameters given in Table 4.

radical anion.[53] Estimates for the geometry of the hydrogen bond were extracted from transient X-band spectra, referring to a protonated sample.[54] Generally, this geometry has only a minor effect on the analysis of the present experiments, performed on a *deuterated* sample.

The ^{15}N hyperfine coupling parameters for P_{700}^{+} were adapted from a recent electron nuclear double resonance (ENDOR) and ESEEM study.[55] Simulations of the ESEEM experiments, performed at multiple microwave frequencies, indicate that the unpaired spin is localized over only one of the two chlorophylls that constitute the primary donor.[55] This is in substantial agreement with a previous ENDOR and ESEEM study, establishing a strongly asymmetric spin density distribution for P_{700}^{+}.[56] The coupling from an axial histidine ligand to P_{700}^{+} has been shown *not* to contribute to the ESEEM modulation pattern.[57] It is therefore reasonable to consider only four ^{15}N hyperfine tensors,[58] whose symmetry axes are collinear (see Table 3). The orientation of this axis in the **g**-tensor system of P_{700}^{+} is characterized by the Euler angles Θ_{1j} and Ψ_{1j} (see Figure 1). Values for these angles can be extracted from the time-dependent X-band spectra of $P_{700}^{+}A_1^{-}$, as demonstrated in Figure 5b. The calculated line shapes refer to a detection time of 200 ns, a fixed value for the angle Θ_{1j} and five different values for the angle Ψ_{1j} ($\Theta_{1j} = 30°$; $\Psi_{1j} = -60°, -30°, 0°, 30°, 60°$). Note the pronounced variation of the spectra with Ψ_{1j}. A similar variation is observed also for the angle Θ_{1j}.

Generally, a set of 27 calculated spectra, selected at various times after the laser pulse, was simultaneously fitted to the experimental spectra by varying the angles Θ_{1j} and Ψ_{1j}. In the calculations, pseudosecular terms for the ^{15}N nuclei were explicitly taken into account.[19,38] The limited resonator bandwidth of 30 MHz was considered by using a Gaussian response function. Similarly, inhomogeneous broadening was taken into account by convolution with a Gaussian of line width $\Delta B_0 = 0.12$ mT.[51] The employed homogeneous spin−spin relaxation time was $T_2 = 1.7$ μs. The dashed lines in Figure 5a represent best simulations, based on the parameter values

$$\Theta_{1j} = 29 \pm 7°$$

$$\Psi_{1j} = 3 \pm 6°$$

Evidently, the agreement achieved is very good. The uniqueness of the fit was tested by running the fit procedure with different starting values. Within the error limits, the same angular values were obtained. Note that these Euler angles[28] characterize the orientation of the symmetry axis of the ^{15}N hyperfine tensors in the **g**-tensor system of P_{700}^{+} (see Table 3). Because of the local character of the hyperfine interactions, it is reasonable to identify this symmetry axis with the chlorophyll normal. Since the statistical errors are reasonably small, we are confident that the extracted chlorophyll orientation is basically correct.

Cofactor Arrangement in the Photosynthetic Membrane. The cofactor arrangement of the secondary radical pair in PSI was determined from angular-dependent W-band spectra, observed for a *magnetically aligned sample* (see Figure 6).[25] Because of the experimental parameters used, that is, a small microwave field and a large time window for signal averaging, a stationary EPR model[10] could be employed in the analysis. Notably, however, *magneto-orientation* by the field of the EPR spectrometer was properly taken into account (see Theory section).[25] The magnetic and structural parameters, used in the

(53) Hales, B. F. *J. Am. Chem. Soc.* **1975**, *97*, 5993−5997.
(54) Link, G.; Bechtold, M.; Schlesselman, S. L.; Thurnauer, M. C.; Kothe, G. Unpublished results.
(55) Mac, M.; Bowlby, N. R.; Babcock, G. T.; McCracken, J. *J. Am. Chem. Soc.* **1998**, *120*, 13215−13223.
(56) Käss, H.; Bittersmann-Weidlich, E.; Andréasson, L.-E.; Bönigk, B.; Lubitz, W. *Chem. Phys.* **1995**, *194*, 419−432.
(57) Mac, M.; Tang, X.-S.; Diner, B. A.; McCracken, J.; Babcock, G. T. *Biochemistry* **1996**, *35*, 13288−13293.
(58) Model calculations indicate that consideration of an additional anisotropic ^{15}N coupling for the histidine ligand has practically no effect on the structural results.

Table 4. Magnetic and Structural Parameters Used in the Simulation of Transient W−Band EPR Experiments of the Light-Induced Radical Pair, P_{700}^{+} A_1^{-}, in Deuterated and ^{15}N-Substituted Photosystem I

microwave field	**g**-tensor components[a] P_{700}^{+}	**g**-tensor components[a] A_1^{-}	spin−spin coupling[b]	inhomogeneous line widths[c]	$\mathbf{g}_1$-tensor orientation[d]	dipolar tensor orientation[d]	susceptibility tensor orient.[e]	orientational order[e]
$\omega/2\pi$ 94.1163 GHz	g_1^X, 2.00311	g_2^X, 2.00624	D, −0.17 mT	$\Delta B_0(P_{700}^{+})$, 0.34 mT	Φ_1, 176°	Φ_D, arbitr.	φ, arbitr.	A, 1.0 ± 0.1
B_1, 0.010 mT	g_1^Y, 2.00256	g_2^Y, 2.00510	E, 0 mT	$\Delta B_0(A_1^{-})$, 0.29 mT	Θ_1, 50°	Θ_D, 78°	ϑ, 81 ± 4°	$S_{Z'Z'}$, 0.13 ± 0.02
	g_1^Z, 2.00230	g_2^Z, 2.00220	J_{ex}, 0 mT		Ψ_1, 64°	Ψ_D, 16°	ψ, 133 ± 6°	

[a] Data from high-field EPR studies.[20,47,48] [b] Parameter values from a recent ESEEM study of $P_{700}^{+}A_1^{-}$.[49] [c] Hyperfine interactions in P_{700}^{+} and A_1^{-} are considered by inhomogeneous Gaussian line widths. [d] Evaluated in the present study from the B_0-dependence of Q-band quantum beat oscillations. The Euler angles[28] relate the principal axis system of the respective magnetic tensor and the magnetic reference system (**g**-tensor of A_1^{-}). [e] Parameter values from the present W-band study on magnetically aligned reaction centers. The listed Euler angles[28] characterize the orientation of the symmetry axis of the susceptibility tensor (membrane normal) in the **g**-tensor system of P_{700}^{+}. The cited errors are linear confidence limits (confidence level 0.95).

W-band simulations, were essentially the same as those employed in the analysis of the X- and Q-band experiments (see Table 4). Hyperfine interactions in P_{700}^{+} and A_1^{-} were considered by inhomogeneous Gaussian line widths. The parameters of the orientational distribution function, ϑ, ψ, and $S_{Z'Z'}$, were determined by simultaneously fitting the two angular-dependent W-band spectra, measured with the director axis either parallel ($\xi = 0°$) or perpendicular ($\xi = 90°$) to the magnetic field. The dashed lines in Figure 6 represent best simulations based on the parameter values

$$\vartheta = 81 \pm 4°$$
$$\psi = 133 \pm 6°$$
$$S_{Z'Z'} = 0.13 \pm 0.02.$$

Generally, the agreement achieved is good. The uniqueness of the fit was tested by running the procedure with different starting values. Within the error limits, the same results were obtained. We are therefore confident that the extracted structural parameters are basically correct.[25] Nevertheless, we expect somewhat larger *systematic* errors due to effects of sequential electron transfer on the spin polarized EPR spectra.[59] These effects become increasingly important at higher magnetic fields.[59]

An order parameter of $S_{Z'Z'} = 0.13$ indicates only partial *magnetic alignment* of the reaction center proteins. This is not surprising in view of the complex biological material, consisting of whole cells of cyanobacteria. The Euler angles ϑ and ψ characterize the orientation of the susceptibility tensor of the proteins embedded in the thylakoid membrane. Theoretical studies indicate that α-helices might be a source of anisotropic diamagnetic susceptibility. [44] In cyanobacterial PSI, a total of 34 transmembrane α-helices are aligned to within a small angle of the membrane normal,[22] which thus represents a natural choice for the principal axis of the susceptibility tensor **Z′** (see Figure 1). Furthermore, any anisotropy in the plane of the membrane will be averaged out for such an arrangement. It is therefore reasonable to identify the symmetry axis of the susceptibility tensor with the membrane normal.[25]

Knowledge of the orientation of the membrane normal in a magnetic reference system makes it possible to depict the cofactor arrangement of $P_{700}^{+}A_1^{-}$ in the photosynthetic membrane, as shown in Figure 7. The structural model describes the orientation of the **g**-tensor of the primary donor, P_{700}^{+}, as well as the position and orientation of the reduced acceptor, A_1^{-}. Note that values for all nine Euler angles, characterizing the geometry of the secondary radical pair, have been obtained

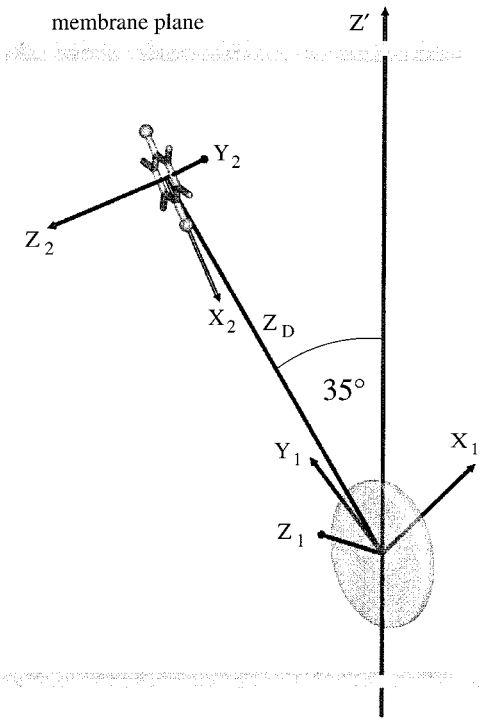

Figure 7. Geometry of the secondary radical pair, $P_{700}^{+}A_1^{-}$, in photosystem I as determined by two-dimensional transient EPR, employing *quantum beat oscillations* (see Tables 1−4). The view direction is parallel to the membrane plane. The shaded disk represents one of the two chlorophyll molecules of the primary donor, which carries the unpaired spin.[55,56] $\mathbf{X}_1$, $\mathbf{Y}_1$, $\mathbf{Z}_1$ = principal axis system of the **g**-tensor of P_{700}^{+}. $\mathbf{X}_2$, $\mathbf{Y}_2$, $\mathbf{Z}_2$ = principal axis system of the **g**-tensor of A_1^{-}. $\mathbf{Z}_D$ = symmetry axis of the dipolar tensor. **Z′** = membrane normal.

(see Tables 1−4). The geometry is based on various two-dimensional EPR experiments, performed at three different microwave frequencies.

Discussion

Recently a second quinone acceptor was located in the X-ray structure of the PSI reaction center protein.[24] Figure 8a depicts a schematic of the cofactor arrangement with respect to the membrane normal, *c*, evaluated from an improved electron density map of PSI at 4 Å resolution.[24] There are two chlorophylls, denoted by eC_1' and eC_1, which constitute the primary donor, P_{700}.[22,24] ENDOR and ESEEM studies indicate that the unpaired spin is basically localized either on eC_1' or eC_1.[55,56] The two quinones, Q_K' and Q_K, are symmetrically positioned on either side of a pseudo-two-fold rotation axis, approximately parallel to the membrane normal.[24] The cofactor arrangement involves

(59) Tang, J.; Bondeson, S.; Thurnauer, M. C. *Chem. Phys. Lett.* **1996**, *253*, 293−298.

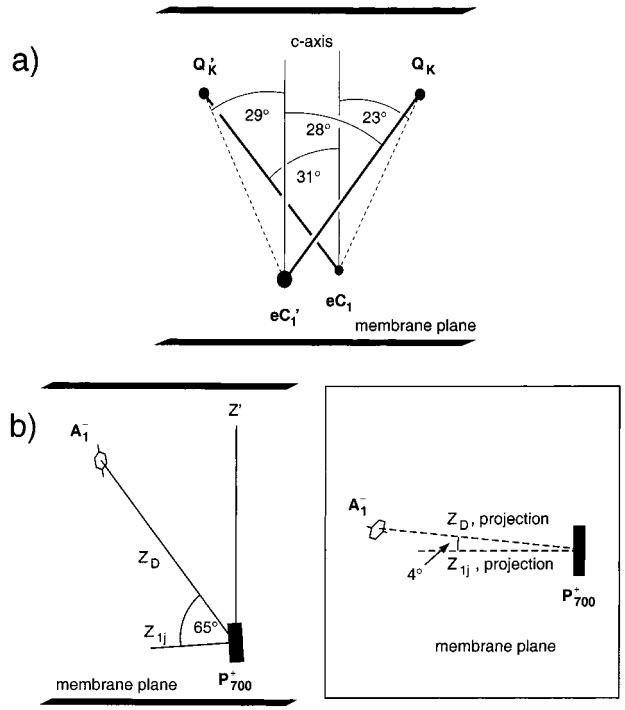

Figure 8. (a) Schematic representation of the cofactor arrangement with respect to the membrane normal, c, evaluated from an electron density map of photosystem I at 4 Å resolution.[24] eC_1', eC_1 = chlorophyll molecules assigned to the primary donor. Q_K', Q_K = quinone acceptors. According to the present study, the cofactor pairs $eC'-Q_K'$ and eC_1-Q_K(dashed lines) are *not* involved in the light-induced electron-transfer process. From the remaining two cofactor pairs (solid lines), $eC_1'-Q_K$ shows the closest correspondence with the charge separated state, $P_{700}^+A_1^-$. (b) Schematic illustration of the geometric parameters used to describe the position of the reduced quinone acceptor, A_1^-, with respect to the primary donor, P_{700}^+ (see Table 6). Left: View direction parallel to the membrane plane. Right: View direction onto the membrane plane. $\mathbf{Z}'$ = membrane normal. $\mathbf{Z}_D$ = $P_{700}^+-A_1^-$ axis. $\mathbf{Z}_{1j}$ = chlorophyll plane normal.

four different donor−acceptor pairs, $eC_1'-Q_K$, eC_1-Q_K', $eC_1'-Q_K'$ and eC_1-Q_K, which can be distinguished by geometric parameters.

These ground-state geometries are the basis for the discussion of the geometry of the charge separated state, $P_{700}^+A_1^-$, evaluated in this study. First, the **g**-tensor orientation of the primary donor is described. Then the structural model for the quinone acceptor is compared with geometric parameters derived from EPR and crystallographic data. Finally, the quinone orientation is discussed in relation to the electron-transfer kinetics of $P_{700}^+A_1^-$, changing significantly at *low temperatures*.[9,60]

Orientation of the g-Tensor of the Primary Donor. As noted above, the orientation of the **g**-tensor, $\mathbf{g}_1$, of P_{700}^+ could be evaluated. To describe this orientation, we define a chlorophyll-based reference system, $\mathbf{X}_{Chl}$, $\mathbf{Y}_{Chl}$, $\mathbf{Z}_{Chl}$, corresponding to the reference system used for the primary donor, P_{865}^+, in purple bacteria:[61] The $\mathbf{Z}_{Chl}$ axis is the chlorophyll normal; the $\mathbf{Y}_{Chl}$ axis is the projection of the membrane normal onto the chlorophyll plane. The $\mathbf{X}_{Chl}$ axis then lies in the chlorophyll plane perpendicular to $\mathbf{Y}_{Chl}$. The angles between the principal axes of $\mathbf{g}_1$ and the molecular reference system can be calculated from the Euler angles characterizing the $P_{700}^+A_1^-$ geometry. They are listed in Table 5 together with the corresponding error limits. Figure 9 depicts a three-dimensional representation of the **g**-tensor orientation of P_{700}^+.

In planar π radicals, such as P_{700}^+, the principal direction corresponding to the smallest **g**-tensor component, g_1^Z, is expected to lie near the normal of the molecular plane.[62] However, inspection of Figure 9 reveals a significant deviation of 29 ±

Table 5. Orientation of the **g**-Tensor of the Primary Donor in Photosystem I[a]

g-tensor axis[b]	chlorophyll based reference system[c] $\mathbf{X}_{Chl}$ (deg)	$\mathbf{Y}_{Chl}$ (deg)	$\mathbf{Z}_{Chl}$ (deg)
$\mathbf{X}_1$	50 ± 6	53 ± 6°	119 ± 7
$\mathbf{Y}_1$	132 ± 6	42 ± 6	89 ± 3
$\mathbf{Z}_1$	68 ± 5	72 ± 5	29 ± 7

[a] Angular values from the present study of the geometry of $P_{700}^+A_1^-$ (see Tables 1−4). The cited errors are based on linear confidence limits (confidence level 0.95). [b] The labeling of the **g**-tensor axes follows common practice, i.e., $g_1^X > g_1^Y > g_1^Z$. [c] The $\mathbf{Z}_{Chl}$ axis is the chlorophyll normal; the $\mathbf{Y}_{Chl}$ axis is the projection of the membrane normal onto the chlorophyll plane; $\mathbf{X}_{Chl}$ then lies in the chlorophyll plane perpendicular to $\mathbf{Y}_{Chl}$.

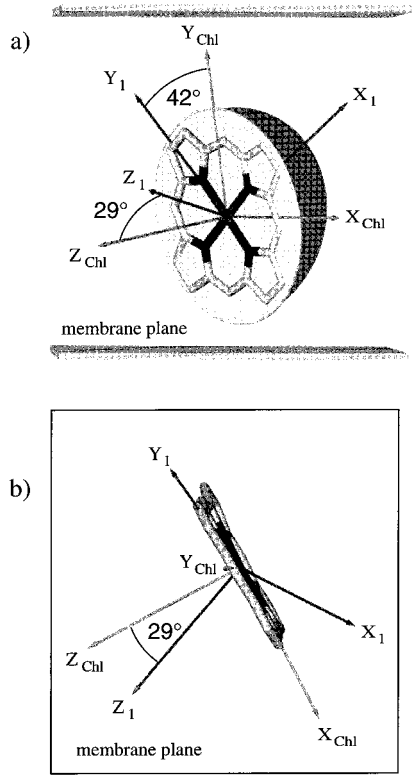

Figure 9. Orientation of the **g**-tensor of the primary donor, P_{700}^+, in photosystem I (see Table 5). The structural information is extracted from two-dimensional transient EPR experiments, employing *quantum beat oscillations*. ENDOR and ESEEM studies indicate that the unpaired spin is localized over only one of the two chlorophylls that constitute the primary donor.[55,56] (a) View direction parallel to the membrane plane. (b) View direction onto the membrane plane. $\mathbf{X}_1$, $\mathbf{Y}_1$, $\mathbf{Z}_1$ = principal axis system of the **g**-tensor of P_{700}^+. $\mathbf{X}_{Chl}$, $\mathbf{Y}_{Chl}$, $\mathbf{Z}_{Chl}$ = chlorophyll based reference system. The $\mathbf{Z}_{Chl}$ axis is the chlorophyll normal; the $\mathbf{Y}_{Chl}$ axis is the projection of the membrane normal onto the chlorophyll plane; the $\mathbf{X}_{Chl}$ axis then lies in the chlorophyll plane perpendicular to $\mathbf{Y}_{Chl}$. The orientation of the chlorophyll molecule in the ($\mathbf{X}_{Chl}$, $\mathbf{Y}_{Chl}$) plane has been chosen according to an X-ray structure of PSI at 4 Å resolution.[24]

(60) Schlodder, E.; Falkenberg, K.; Gergeleit, M.; Brettel, K. *Biochemistry* **1998**, *37*, 9466−9476.

(61) Klette, R.; Törring, J. T.; Plato, M.; Möbius, K. *J. Phys. Chem.* **1993**, *97*, 2015−2020.

(62) Stone, A. J. *Mol. Phys.* **1963**, *7*, 311−316.

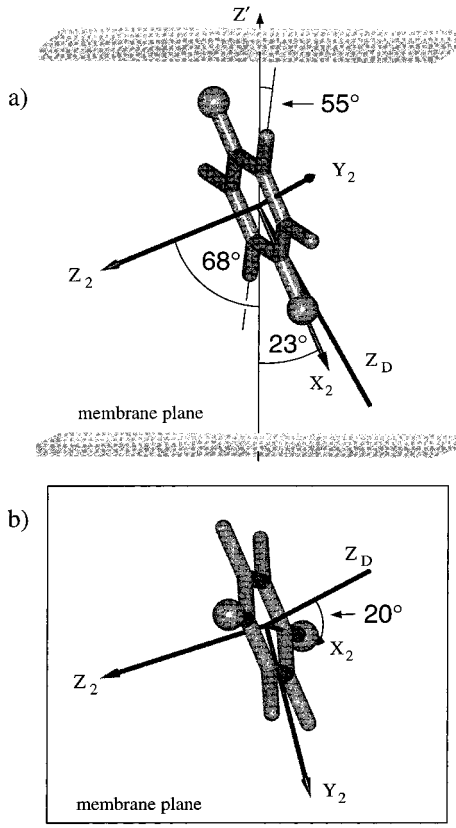

Figure 10. Structural model for the reduced quinone acceptor, A_1^-, in photosystem I as determined from *low temperature* transient EPR experiments, employing *quantum beat oscillations* (see Table 6). (a) View direction parallel to the membrane plane. (b) View direction onto the membrane plane. $\mathbf{X}_2$ = quinone O−O axis. $\mathbf{Y}_2$ = phylloquinone long axis. $\mathbf{Z}_2$ = quinone plane normal. $\mathbf{Z}_D$ = symmetry axis of the dipolar tensor. $\mathbf{Z}'$ = membrane normal.

7° between $\mathbf{Z}_1$ and $\mathbf{Z}_{Chl}$.[63,64] In view of the monomeric character of P_{700}^+,[55,56] such a deviation is surprising. Possibly, neighboring pigments or ligating amino acids[57] are responsible for this deviation. The corresponding value for the **g**(1)-tensor orientation of P_{865}^+ in purple bacteria is 38°.[61] Figure 9 further shows that the $\mathbf{Y}_1$ axis lies in the chlorophyll plane, forming an angle of 42 ± 6° with the $\mathbf{Y}_{Chl}$ axis (see Table 5). Similar is true for the **Y**(1) axis of the **g**(1)-tensor in purple bacteria where the corresponding angle amounts to 32°.[61] Evidently, there is a close similarity between the **g**-tensor orientation of P_{700}^+ in PSI and the **g**(1)-tensor orientation of P_{865}^+ in purple bacteria.[61]

Structural Model for the Quinone Acceptor. Figure 10 shows a structural model for the reduced quinone acceptor based on the Euler angles evaluated in this study. The model is quantified by the geometric parameters summarized in Table 6. In the following, the parameter values are compared with the corresponding values from recent EPR and crystallographic studies based on PSI single crystals or oriented PSI particles.

Our EPR results indicate that the quinone plane of A_1^- is inclined by 68 ± 7° relative to the membrane plane (see Figure 10a). This compares favorably with a value of 76 ± 10° obtained by CW EPR using oriented PSI particles.[48] The angle between the quinone O−O axis and the membrane normal (see Figure 10a) is found to be 23 ± 7°, in excellent agreement with previous EPR spectroscopic values of 25−30°[23] and 27 ± 10°.[48] In the present model, the quinone O−O axis is found to be inclined by 20 ± 3° relative to the $P_{700}^+-A_1^-$ axis (see Figure 10b). This angle was put to 0 ± 5° by previous EPR simulations.[20,23] Evidently, the match between the two EPR values is less satisfactory. It should be noted, however, that a value of 0° does not well reproduce the low-field transients of the two-dimensional Q-band experiment. In our model, the methyl group of the quinone faces either the lumen or the stroma, while the C_2-C_{methyl} axis forms an angle of 55 ± 6° with the membrane normal (see Figure 10a). This value is in substantial agreement with an estimate of 35−55°, obtained by transient EPR using PSI single crystals.[23]

In the X-ray structure of PSI at 4 Å resolution, the *orientation of the quinones* mostly remains undetermined.[24] Consequently, the four geometric parameters, discussed so far, do not aid in assigning $P_{700}^+ A_1^-$ to a particular cofactor pair (see Figure 8a). In contrast, the following three parameters, characterizing the *position of the quinones* in the electron-transfer system, may be used for this purpose. The inclination angle of the $P_{700}^+-A_1^-$ axis relative to the membrane normal (see Figure 7) is found to be 35 ± 6°. This value agrees satisfactorily with an EPR spectroscopic value of 27 ± 5°, used to locate the quinone acceptor in the electron-transfer system of PSI.[21] The result is corroborated by other recent EPR studies.[23,65] The corresponding crystallographic values for $eC_1'-Q_K$, eC_1-Q_K', $eC_1'-Q_K'$, and eC_1-Q_K are 28 ± 3°, 31 ± 3°, 29 ± 3°, and 23 ± 3°.[24] Here, only $eC_1'-Q_K$, eC_1-Q_K', and $eC_1'-Q_K'$ yield satisfactory agreement, whereas eC_1-Q_K can be eliminated.

In the present EPR model, the angle between the chlorophyll normal and the $P_{700}^+-A_1^-$ axis, both projected onto the membrane plane (see Figure 8b), is found to be 4 ± 11°. This value has to be compared with crystallographic values of 5 ± 5°, 3 ± 5°, 39 ± 5°, and 29 ± 5° for $eC_1'-Q_K$, eC_1-Q_K', $eC_1'-Q_K'$, and eC_1-Q_K, respectively.[24] Clearly, $eC_1'-Q_K$ and eC_1-Q_K' (see solid lines in Figure 8a) both show an excellent correspondence to the EPR result. On the other hand, the cofactor pairs $eC_1'-Q_K'$ and eC_1-Q_K (see dashed lines in Figure 8a) can be ruled out for the assignment of $P_{700}^+A_1^-$. In our model, the angle between the chlorophyll plane normal and the $P_{700}^+-A_1^-$axis (see Figure 8b) is found to be 65 ± 5°. The crystallographic values for the two remaining cofactor pairs $eC_1'-Q_K$ and eC_1-Q_K' are 66 ± 5°and 53 ± 5°. Clearly, $eC_1'-Q_K$ shows the closest correspondence with $P_{700}^+A_1^-$. This suggests *unidirectional electron transfer* via the quinone Q_K, which only lately has been located in the X-ray structure of PSI.[24] On the other hand, also eC_1-Q_K' mostly remains within the error limits of both methods. Thus, electron transfer along eC_1-Q_K' cannot *entirely* be excluded.

Evidently, at *low temperatures* the geometry of $P_{700}^+A_1^-$ is compatible with the ground-state structure as obtained by X-ray crystallography.[24] It should be noted, however, that under the experimental conditions (70 K, glycerol as cryoprotection), the observed intermediate has a lifetime of about 150 μs and decays by *charge recombination*.[9,60] A somewhat different geometry for $P_{700}^+A_1^-$ has been extracted from time-resolved X-band measurements performed at *room temperature*,[18] where $P_{700}^+A_1^-$ decays in about 200 ns by *forward electron transfer* to the FeS centers.[4,7,8,66] We have repeated this *room-temperature* EPR experiment by circulating the sample through a quartz capillary

(63) After the present paper was submitted, it came to our notice that Zech et al. have just reported an even larger tilt angle of 43°between $\mathbf{Z}_1$ and $\mathbf{Z}_{Chl}$ for P_{700}^+ (ref 64).

(64) Zech, S. G.; Hofbauer, W.; Kamlowski, A.; Fromme, P.; Stehlik, D.; Lubitz, W.; Bittl, R. *J. Phys. Chem. B* **2000**, *104*, 9728−9739.

(65) Yoshii, T.; Hara, H.; Kawamuri, A.; Akabori, K.; Iwaki, M.; Itoh, S. *Appl. Magn. Reson.* **1999**, *16*, 565−580.

(66) Bock, C. H.; van der Est, A. J.; Brettel, K.; Stehlik, D. *FEBS Lett.* **1989**, *247*, 91−96.

Table 6. Geometric Parameters Characterizing the Orientation and Position of the Quinone Acceptor in Photosystem I

	transient EPR[b] this work	pulsed EPR[c] single crystals	transient EPR[d] single crystals	CW EPR[e] oriented sample	X-ray crystallography[f]			
geometric parameters[a]	$P_{700}^{+}A_1^{-}$ (deg)	$P_{700}^{+}A_1^{-}$ (deg)	$P_{700}^{+}A_1^{-}$ (deg)	$P_{700}^{+}A_1^{-}$ (deg)	$eC_1'-Q_K$ (deg)	eC_1-Q_K' (deg)	$eC_1'-Q_K'$ (deg)	eC_1-Q_K (deg)
$<(\mathbf{Z}; \mathbf{Z}')$	68 ± 7			76 ± 10				
$<(\mathbf{X}_2; \mathbf{Z}')$	23 ± 7		25−30	27 ± 10				
$<(\mathbf{X}_2; \mathbf{Z}_D)$	20 ± 3		0 ± 5					
$<(\mathbf{Z}_{21}; \mathbf{Z}')$	55 ± 6		35−55					
$<(\mathbf{Z}_D; \mathbf{Z}')$	35 ± 6	27 ± 5	27 ± 10		28 ± 3	31 ± 3	29 ± 3	23 ± 3
$<(\mathbf{Z}_{1j}, \mathbf{Z}_D;$ both projected onto the membrane plane)	4 ± 11				5 ± 5	3 ± 5	39 ± 5	29 ± 5
$<(\mathbf{Z}_{1j}; \mathbf{Z}_D)$	65 ± 5				66 ± 5	53 ± 5	64 ± 5	76 ± 5

[a] The assignment of the axes is given in Figure 1. $\mathbf{Z}_2$ = quinone plane normal, $\mathbf{Z}'$ = membrane normal, $\mathbf{X}_2$ = quinone O−O axis, $\mathbf{Z}_D = P_{700}^{+} - A_1^{-}$ axis, $\mathbf{Z}_{21} = C_2-C_{methyl}$ axis, $\mathbf{Z}_{1j}$ = chlorophyll plane normal (see Figures 7−10). [b] Values calculated from the Euler angles characterizing the geometry of $P_{700}^{+}A_1^{-}$ (see Tables 1−4). The cited errors are based on linear confidence limits (confidence level 0.95). [c] Adapted from an ESEEM study of $P_{700}^{+}A_1^{-}$ in PSI single crystals.[21] [d] Values from a transient EPR study of $P_{700}^{+}A_1^{-}$ in PSI single crystals.[23] [e] Adapted from a CW EPR study of A_1^{-} in oriented multilayers of PSI.[48] [f] Data from an X-ray structure of PSI at 4 Å resolution.[24]

located in the microwave resonator. Analysis of the observed *quantum beats* on the basis of *fast forward electron transfer* indicates that the orientation of the reduced quinone acceptor, A_1^{-}, is different at *room temperature* than at *low temperature*. In view of the limited spectral resolution of the X-band experiment, however, this challenging result has to be checked by time-resolved EPR investigations at higher microwave frequencies. Studies along these lines are currently in progress.

Conclusions

We have evaluated the three-dimensional structure of the short-lived radical pair intermediate $P_{700}^{+}A_1^{-}$ following photoexcitation of PSI in its native membrane. Thus, we also obtain the cofactor arrangement of $P_{700}^{+}A_1^{-}$ with respect to the membrane. The structure describes the orientation of the **g**-tensor of the primary donor, P_{700}^{+}, as well as the position and orientation of the reduced acceptor, A_1^{-}. The new structural information is based on the analysis of *quantum beat oscillations* in combination with multifrequency EPR and a *magnetically oriented sample*.

With these techniques, it is possible to evaluate the geometry of the transient intermediates over a wide temperature range. Preliminary *room-temperature* studies of $P_{700}^{+}A_1^{-}$ suggest that the orientation of the reduced quinone acceptor is different from that at *low temperatures*, where *forward electron transfer* to the FeS centers is partially blocked. This challenging result may help in understanding how the quinone acceptor functions in PSI.

Finally, we have demonstrated that the complementary information obtained from *quantum beats* observed at different microwave frequencies is a powerful structural tool. We expect that this is of general interest, particularly to researchers in the broad fields related to solar energy conversion and storage, since the detailed structure of radical pair intermediates can be determined on a nanosecond time scale.

Acknowledgment. We thank Ulrich Heinen (University of Freiburg) for helpful discussions and advice. Financial support by the Deutsche Forschungsgemeinschaft (Ko/16-3; Schwerpunktprogramm Hochfeld-EPR) is gratefully acknowledged. Work at Argonne National Laboratory was supported by the U.S. Department of Energy, Office of Basic Energy Sciences, Division of Chemical Sciences (Contract W-31-109-ENG-38). Most of the numerical calculations were carried out on a SGI Origin 2000 at the computer center of the University of Freiburg.

JA003382H